

Entropy, fidelity, and double orthogonality for resonance states in two-electron quantum dots

Federico M. Pont,^{*} Omar Osenda,[†] and Pablo Serra[‡]

*Facultad de Matemática, Astronomía y Física,
Universidad Nacional de Córdoba, and IFEG-CONICET,
Ciudad Universitaria, X5016LAE Córdoba, Argentina*

Julio H. Toloza[§]

*Universidad Nacional del Nordeste, Avenida Libertad 5400,
W3404AAS Corrientes, Argentina and
IMIT-CONICET*

(Dated: October 14, 2018)

Abstract

Resonance states of a two-electron quantum dot are studied using a variational expansion with both real basis-set functions and complex scaling methods. The two-electron entanglement (linear entropy) is calculated as a function of the electron repulsion at both sides of the critical value, where the ground (bound) state becomes a resonance (unbound) state. The linear entropy and fidelity and double orthogonality functions are compared as methods for the determination of the real part of the energy of a resonance. The complex linear entropy of a resonance state is introduced using complex scaling formalism.

PACS numbers: 31.15.ac,03.67.Mn,73.22.-f

^{*}Electronic address: pont@famaf.unc.edu.ar

[†]Electronic address: osenda@famaf.unc.edu.ar

[‡]Electronic address: serra@famaf.unc.edu.ar

[§]Electronic address: jtoloza@exa.unne.edu.ar

I. INTRODUCTION

In the past few years the application of quantum information concepts to some long standing problems has led to a deeper understanding of those problems [1] and, as a consequence, to the formulation of new methods to solve (or calculate) them. For example, the simulability of many body problems is determined by the amount of entanglement shared between the spins of the system [2].

There is a number of quantities that can be calculated in order to analyze the information carried by a given state including the entanglement of formation [3], the fidelity [4] and several kinds of entropies, entanglement witnesses and so on. Of course it depends on the problem which quantity is more adequate, or accessible, to be calculated.

In the case of atomic or few body systems with continuous degrees of freedom a rather natural quantity is the von Neumann entropy, it has been used to study a number of problems: Helium like atom [5], [6], generation of entanglement via scattering [7], the dynamical entanglement of small molecules [8], and entanglement in Hooke's atom [9].

In quantum dots, most quantum information studies focus in the amount of entanglement carried by its eigenstates [10, 11], or in the controllability of the system [12]. Both approaches are driven by the possible use of a quantum dot as the physical realization of a qubit[13]. The controllability of the system is usually investigated (or performed) between the states with the lowest lying eigenenergies [14].

Besides the possible use of quantum dots as quantum information devices there are proposals to use them as photodetectors. The proposal is based on the use of resonance states because of its properties, in particular its large scattering section compared to the scattering sections of bounded states [16].

The resonance states are slowly decaying scattering states characterized by a large but finite lifetime. Resonances are also signaled by sharp, Lorentzian-type peaks in the scattering matrix. In many cases of interest where complex scaling (analytic dilatation) techniques can be applied, resonances energies show up as isolated complex eigenvalues of the rotated Hamiltonian [15]. Under this transformation the bound states remain exactly preserved and the resonance states are exposed as \mathcal{L}^2 functions of the rotated Hamiltonian. Resonance states can be observed in two-electron quantum dots [16, 17] and two-electron atoms [18].

Recently, a work by Ferrón, Osenda, and Serra [19] studied the behavior of the von

Neumann entropy associated with \mathcal{L}^2 approximations of resonance states of two electron quantum dots. In particular that work was focused in the resonance state that arises when the ground state loses its stability, *i.e.* the quantum dot does not have two electron bounded states any more. Varying the parameters of the quantum dot allows the energy to cross the ionization threshold that separates the region where the two electron ground state is stable from the region where the quantum dot loses one electron.

In reference [19] it was found that the von Neumann entropy provide a way to obtain the real part of the energy of the resonance, in other words, the von Neumann entropy provides a stabilization method. The numerical approximation used in [19] allowed to obtain only a reduced number of energy levels (in a region where the spectrum is continuous) their method provided the real part of the energy of the resonance only for a discrete set of parameters and this set could not be chosen *a priori*. Notwithstanding this, Ferrón *et al.*, conjectured that there is a well defined function $S(E_r)$, the von Neumann entropy of the resonance state, which has a well defined value for every value of the real part of the energy of the resonance, E_r .

In this work we will show, if λ is the external parameter that drives the quantum dot through the ionization threshold, that the entropy $S(E_r(\lambda))$ is a smooth function of λ . Also it is showed that the resonance state entropy calculated by Ferrón *et al.* is correct near the ionization threshold.

We have studied other quantities, besides the entropy, that are good witnesses of resonance presence. One of them is the Fidelity, which has been widely used [20, 20–22] in the detection of non-analytical behavior in the spectrum of quantum systems. The analysis of the Fidelity provides a method to obtain the real part of the resonance energy from variational eigenstates. We introduce the *Double Orthogonality* function (DO) that measures changes in quantum states and detects the resonance region. The DO compares the extended continuum states and the state near the resonance, also providing the real part of the resonance energy.

The paper is organized as follows. In Section II we present the model and briefly explain the technical details to obtain approximate eigenvalues, eigenfunctions, and the density of states for the problem. In Section III the fidelity is used to obtain the real part of the resonance energy and the Double Orthogonality is introduced as an alternative method. In Section IV the linear entropy and the expectation value of the Coulombian repulsion are

studied using complex scaling methods. Finally, in Section V we discuss our results and present our conclusions.

II. THE MODEL AND BASIC RESULTS

There are many models of quantum dots, with different symmetries and interactions. In this work we consider a model with spherical symmetry, with two electrons interacting via the Coulomb repulsion. The main results should not be affected by the particular potential choice as it is already known that the near threshold behavior and other critical quantities (such as the critical exponents of the energy and other observables) are mostly determined by the range of the involved potentials [24]. Therefore to model the dot potential we use a short-range potential suitable to apply the complex scaling method. After this considerations we propose the following Hamiltonian H for the system

$$H = -\frac{\hbar^2}{2m}\nabla_{\mathbf{r}_1}^2 - \frac{\hbar^2}{2m}\nabla_{\mathbf{r}_2}^2 + V(r_1) + V(r_2) + \frac{e^2}{|\mathbf{r}_2 - \mathbf{r}_1|}, \quad (1)$$

where $V(r) = -(V_0/r_0^2) \exp(-r/r_0)$, \mathbf{r}_i the position operator of electron $i = 1, 2$; r_0 and V_0 determine the range and depth of the dot potential. After re-scaling with r_0 , in atomic units the Hamiltonian of Eq. (1) can be written as

$$H = -\frac{1}{2}\nabla_{\mathbf{r}_1}^2 - \frac{1}{2}\nabla_{\mathbf{r}_2}^2 - V_0 e^{-r_1} - V_0 e^{-r_2} + \frac{\lambda}{|\mathbf{r}_2 - \mathbf{r}_1|}, \quad (2)$$

where $\lambda = r_0$.

We choose the exponential binding potential to take advantage of its analytical properties. In particular this potential is well behaved and the energy of the resonance states can be calculated using complex scaling methods. So, besides its simplicity, the exponential potential allows us to obtain independently the energy of the resonance state and a check for our results. The threshold energy, ε , of Hamiltonian Eq. (2), that is, the one body ground state energy can be calculated exactly [25] and is given by

$$J_{2\sqrt{2\varepsilon}}(\sqrt{2V_0}) = 0, \quad (3)$$

where $J_\nu(x)$ is the Bessel function.

The discrete spectrum **and** the resonance states of the model given by Eq. (2) can be obtained approximately using \mathcal{L}^2 variational functions [17], [23]. So, if $|\psi_j(1,2)\rangle$ are the exact eigenfunctions of the Hamiltonian, we look for variational approximations

$$|\psi_j(1, 2)\rangle \simeq |\Psi_j(1, 2)\rangle = \sum_{i=1}^M c_i^{(j)} |\Phi_i\rangle, \quad c_i^{(j)} = (\mathbf{c}^{(j)})_i; \quad j = 1, \dots, M. \quad (4)$$

where the $|\Phi_i\rangle$ must be chosen adequately and M is the basis set size.

Since we are interested in the behavior of the system near the ground-state ionization threshold, we choose as basis set s-wave singlets given by

$$|\Phi_i\rangle \equiv |n_1, n_2; l\rangle = (\phi_{n_1}(r_1) \phi_{n_2}(r_2))_s \mathcal{Y}_{0,0}^l(\Omega_1, \Omega_2) \chi_s, \quad (5)$$

where $n_2 \leq n_1$, $l \leq n_2$, χ_s is the singlet spinor, and the $\mathcal{Y}_{0,0}^l(\Omega_1, \Omega_2)$ are given by

$$\mathcal{Y}_{0,0}^l(\Omega_1, \Omega_2) = \frac{(-1)^l}{\sqrt{2l+1}} \sum_{m=-l}^l (-1)^m Y_{lm}(\Omega_1) Y_{l-m}(\Omega_2), \quad (6)$$

i.e. they are eigenfunctions of the total angular momentum with zero eigenvalue and the Y_{lm} are the spherical harmonics. Note also that $\mathcal{Y}_{0,0}^l$ is a real function since it is symmetric in the particle index. The radial term $(\phi_{n_1}(r_1)\phi_{n_2}(r_2))_s$ has the appropriate symmetry for a singlet state,

$$(\phi_{n_1}(r_1)\phi_{n_2}(r_2))_s = \frac{\phi_{n_1}(r_1)\phi_{n_2}(r_2) + \phi_{n_1}(r_2)\phi_{n_2}(r_1)}{[2(1 + \langle n_1|n_2\rangle^2)]^{1/2}} \quad (7)$$

where

$$\langle n_1|n_2\rangle = \int_0^\infty r^2 \phi_{n_1}(r) \phi_{n_2}(r) dr, \quad (8)$$

and the ϕ 's are chosen to satisfy $\langle n_1|n_1\rangle = 1$. The numerical results are obtained by taking the Slater type forms for the orbitals

$$\phi_n^{(\alpha)}(r) = \left[\frac{\alpha^{2n+3}}{(2n+2)!} \right]^{1/2} r^n e^{-\alpha r/2}. \quad (9)$$

where α is a non-linear parameter of the basis. It is clear that in terms of the functions defined in Eq. (5) the variational eigenfunctions reads as

$$\left| \Psi_i^{(\alpha)}(1, 2) \right\rangle = \sum_{n_1 n_2 l} c_{n_1 n_2 l}^{(i), (\alpha)} |n_1, n_2; l; \alpha\rangle, \quad (10)$$

where $n_1 \geq n_2 \geq l \geq 0$, then the basis set size is given by

$$M = \sum_{n_1=0}^N \sum_{n_2=0}^{n_1} \sum_{l=0}^{n_2} 1 = \frac{1}{6} (N+1)(N+2)(N+3), \quad (11)$$

so we refer to the basis set size using both N and M . In Eq. (10) we added α as a basis index to indicate that in general the variational eigenfunction is α -dependent. The matrix elements of the kinetic energy, the Coulombic repulsion between the electrons and other mathematical details involving the functions $|n_1, n_2; l; \alpha\rangle$ are given in references [26], [27]. We only show here for completeness the matrix elements of the exponential potential in the basis of Eq. (9),

$$\langle n | e^{-r} | n' \rangle = \int_0^\infty \phi_n(r) \phi_{n'}(r) e^{-r} r^2 dr = \left(\frac{\alpha}{1+\alpha} \right)^{n+n'+3} \frac{(2+n+n')!}{\sqrt{(2n+2)!(2n'+2)!}}. \quad (12)$$

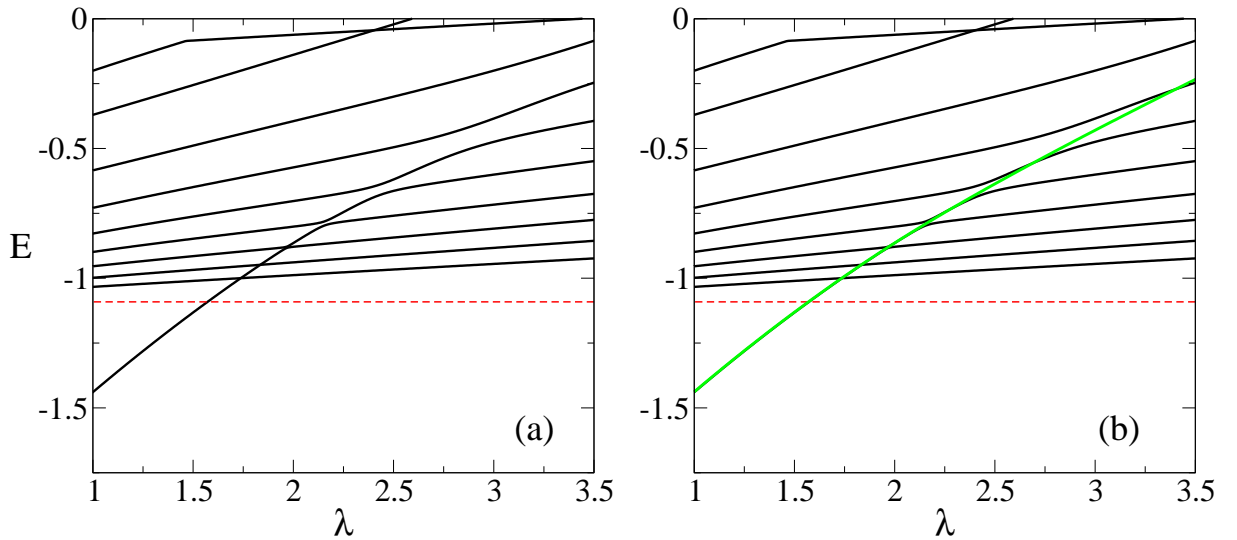


FIG. 1: (color on-line) (a) the figure shows the behavior of the variational eigenvalues $E_j^{(\alpha)}(\lambda)$ (black lines) for $N = 14$ and non-linear parameter $\alpha = 2$. The red dashed line corresponds to the threshold energy $\varepsilon \simeq -1.091$. Note that the avoided crossings between the variational eigenvalues are fairly visible. (b) The figure shows the same variational eigenvalues that (a) (black lines) and the energy calculated using the complex scaling method (green line) for a parameter $\theta = \pi/10$.

Resonance states have isolated complex eigenvalues, $E_{res} = E_r - i\Gamma/2$, $\Gamma > 0$, whose eigenfunctions are not square-integrable. These states are considered as quasi-bound states of energy E_r and inverse life time Γ . For the Hamiltonian Eq. (2), the resonance energies belong to the interval $(\varepsilon, 0)$ [15].

The resonance states can be analyzed using the spectrum obtained with a basis of \mathcal{L}^2 functions (see [19] and References therein). The levels above the threshold have several

avoided crossings that “surround” the real part of the energy of the resonance state. The presence of a resonance can be made evident looking at the eigenvalues obtained numerically. Figure 1 shows a typical spectrum obtained from the variational method. This figure shows the behavior of the variational eigenvalues $E_j^{(\alpha)}$ as functions of the parameter λ . The results shown were obtained using $N = 14$ and $\alpha = 2.0$. The value of α was chosen in order to obtain the best approximation for the energy of the ground state in the region of λ where it exists. The Figure shows clearly that for $\lambda < \lambda_{th} \simeq 1.54$ there is only one bounded state. Above the threshold the variational approximation provides a finite number of solutions with energy below zero. Above the threshold there is not a clear cut criteria to choose the value of the variational parameter. However, it is possible to calculate $E_r(\lambda)$ calculating $E_j^{(\alpha)}$ for many different values of the variational parameter (see Kar and Ho [28]).

Figure 2 (a) and (b) shows the numerical results for the first and second eigenvalues respectively, for different values of the variational parameter α . The figure also shows the behavior of the ground state (below the threshold) and the real part of the energy of the resonance calculated using complex scaling (above the threshold), this curve is used as a reference. The behavior of the smaller variational eigenvalue $E_1^{(\alpha)}(\lambda)$ is rather clear, below the threshold $E_1^{(\alpha)}(\lambda)$ is rather insensitive to the actual value of α , the differences between $E_1^{(\alpha=2)}(\lambda)$ and $E_1^{(\alpha=6)}(\lambda)$ are smaller than the width of the lines shown in the figure. Above the threshold the behavior changes, the curve for a given value of α has two well defined regions, in each region E_1 is basically a straight line. The two straight lines in each region has a different slope and the change in the slope is located around $E_r(\lambda)$.

In the case of $E_2^{(\alpha)}(\lambda)$ there are three regions, in each one of them the curve for a given value of α is basically a straight line and the slope is different in each region. A feature that appears rather clearly is that, for fixed λ , the density of levels for energy unit is not uniform, despite that the curves $E_j^{(\alpha_i)}(\lambda)$ are drawn for forty equally spaced α_i 's between $\alpha = 2.0$ and $\alpha = 6.0$. This fact has been observed previously [33] and the density of states can be written in terms of two contributions, a localized one and an extended one. The localized density of states is attributed to the presence of the resonance state, conversely the extended density of states is attributed to the continuum of states between $(\varepsilon, 0)$.

The localized density of states $\rho(E)$ can be expressed as [28, 33]

$$\rho(E) = \left| \frac{\partial E(\alpha)}{\partial \alpha} \right|^{-1}. \quad (13)$$

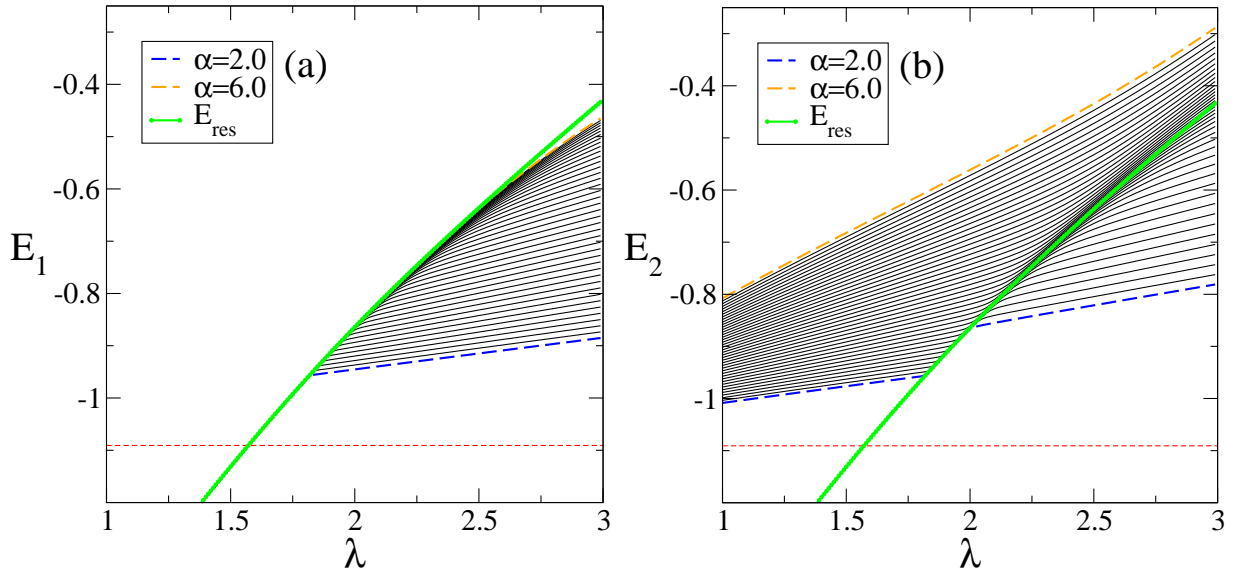


FIG. 2: (color on-line) (a) The first variational state energy *vs* λ , for different values of the variational parameter α . From bottom to top α increases its value from $\alpha = 2$ (dashed blue line) to $\alpha = 6$ (dashed orange line). The real part of the resonance eigenvalue obtained using complex scaling ($\theta = \pi/10$) is also shown (green line). (b) Same as (a) but for the second state energy.

Since we are dealing with a variational approximation, we calculate

$$\rho(E_j^{(\alpha_i)}(\lambda)) = \left| \frac{E_j^{(\alpha_{i+1})}(\lambda) - E_j^{(\alpha_{i-1})}(\lambda)}{\alpha_{i+1} - \alpha_{i-1}} \right|^{-1}. \quad (14)$$

Figure 3 shows the typical behavior of $\rho_j(E) \equiv \rho(E_j^{(\alpha_i)}(\lambda))$ for several eigenenergies and $\lambda = 2.25$. The real and imaginary parts of the resonance's energy, $E_r(\lambda)$ and Γ respectively, can be obtained from $\rho(E)$, see for example [28] and references there in. This method provides an independent way to obtain E_{res} , besides the method of complex scaling.

The values of $E_r(\lambda)$ and $\Gamma(\lambda)$ are obtained performing a nonlinear fitting of $\rho(E)$, with a Lorentzian function,

$$\rho(E) = \rho_0 + \frac{A}{\pi} \frac{\Gamma/2}{[(E - E_r)^2 + (\Gamma/2)^2]}. \quad (15)$$

One of the drawbacks of this method results evident: for each λ there are several $\rho_j(E)$ (in fact one for each variational level), and since each $\rho_j(E)$ provides a value for $E_r^j(\lambda)$ and $\Gamma^j(\lambda)$ one has to choose which one is the best. Kar and Ho [28] solve this problem fitting all the $\rho_j(E)$ and keeping as the best values for $E_r(\lambda)$ and $\Gamma(\lambda)$ the fitting parameters with the

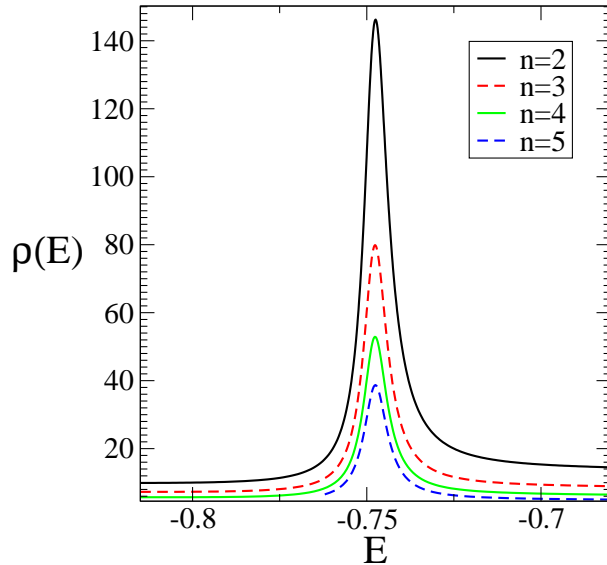


FIG. 3: (color on-line) The density of states $\rho(E)$ for $\lambda = 2.25$ and basis set size $N = 14$. The results were obtained using Eq. (13) and correspond to, from top to bottom, the second (black line), third (dashed red line), fourth (green line) and fifth (dashed blue line) levels.

smaller χ^2 value. At least for their data the best fitting (the smaller χ^2) usually corresponds to the larger n . This fact has a clear interpretation, if the numerical method approximates $E_r(\lambda)$ with $E_n^{(\alpha)}(\lambda)$ a large n means that the numerical method is able to provide a large number of approximate levels, and so the continuum of states between $(\varepsilon, 0)$ is “better” approximated.

It is worth to remark that the results obtained from the complex scaling method and from the density of states are in excellent agreement, see Table I.

III. FIDELITY AND DOUBLE ORTHOGONALITY FUNCTIONS

Since the work of Zanardi et al. [20, 21] there has been a growing interest in the fidelity approach as a mean to study quantum phase transitions [20], the information-theoretic differential geometry on quantum phase transitions (QPT’s) [21] or the disordered quantum XY model [22]. In all these cases the fidelity is used to detect the change of behavior of the states of a quantum system. For example, if λ is the external parameter that drives a system through a QPT, the fidelity is the superposition $\mathcal{F} = \langle \Psi(\lambda - \delta\lambda), \Psi(\lambda + \delta\lambda) \rangle$, where Ψ is the ground state of the system. It has been shown that \mathcal{F} is a good detector of critical

behavior in ordered [20] and disordered systems[22].

In the following we will show that the energy levels calculated using the variational approximation show critical behavior near the energy of the resonance, moreover the curve $E_r(\lambda)$ can be obtained from the fidelity.

Figure 4 shows the behavior of the function $\mathcal{G}_n = 1 - F_n$, where $F_n = |\langle \Psi_n(\lambda), \Psi_n(\lambda + \delta\lambda) \rangle|^2$, and Ψ_n is the n^{th} eigenstate obtained with the variational approach.

The behavior of \mathcal{G} is quite simple. The value of \mathcal{G} is very small, except near the avoided crossings where the value of \mathcal{G} increases rather steeply (at least for small n). This is so because near the avoided crossing the superposition $|\langle \Psi_n(\lambda), \Psi_n(\lambda + \delta\lambda) \rangle|^2 \rightarrow 0$. Actually, $|\langle \Psi_n(\lambda), \Psi_n(\lambda + \delta\lambda) \rangle|^2 \rightarrow 0$ near points such that $E_n^{(\alpha)}(\lambda)$ has non analytical behavior. Is for this reason that the fidelity is a good detector of quantum phase transitions [20–22]. In a first order QPT the energy of the ground state is non analytical, and in a second order QPT the gap in the avoided crossing between the ground state and the first excited state goes to zero in the thermodynamic limit.

The previous argument supports why \mathcal{G}_1 has only one peak, while all the others functions \mathcal{G}_n have two peaks, the number of peaks is the number of avoided crossings of each level. However, since the resonance state lies somewhere between the avoided crossings it is natural to ask what feature of the fidelity signals the presence of the resonance. For a given level n the value of the energy is fixed, so we must pick a distinctive feature of \mathcal{G}_n that is present for some λ_n^f , such that $E_r(\lambda_n^f) \simeq E_n(\lambda_n^f)$ (from here we will use E_n or $E_n^{(\alpha)}$ interchangeably). It results to be, that λ_n^f is the value of λ such that \mathcal{G}_n attains its minimum between its two peaks. Figure 4 shows the points $E_n(\lambda_n^f)$. In Table I we tabulate the real part of the energy calculated using DO, complex scaling, fidelity and Density of States, for the five values of λ_n^f shown in Figure 4. The numerical values obtained using the fidelity and Density of States methods are identical up to five figures. The Relative Error between the energies obtained is less than 0.25%

The idea of detecting the resonance state energy with functions depending on the inner product could be taken a step further. To this end we consider the functions

$$DO_n(\lambda) = |\langle \Psi_n(\lambda_L), \Psi_n(\lambda) \rangle|^2 + |\langle \Psi_n(\lambda_R), \Psi_n(\lambda) \rangle|^2, \text{ for } \lambda_L < \lambda < \lambda_R \quad (16)$$

where λ_L and λ_R are two given coupling values. It is clear from the definition that

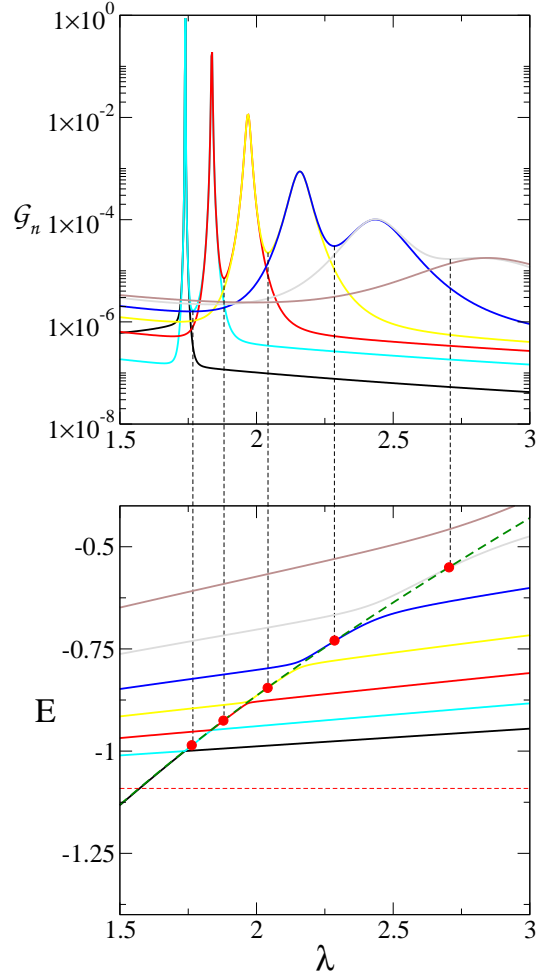


FIG. 4: (color on-line) The upper panel shows the behavior of \mathcal{G}_n , for $n = 1, \dots, 7$. Each function \mathcal{G}_n has two peaks, except for $n = 1$. Since one of the peaks of \mathcal{G}_n coincides with one of the peaks of \mathcal{G}_{n+1} , only one peak for each level n is apparent. From left to right the visible line at each peak correspond to $n = 2, \dots, 7$ (cyan, red, yellow, blue, grey, brown lines, respectively). The $n = 1$ line has no visible peak (black). The lower panel shows the variational eigenlevels $n = 1, \dots, 7$ (with the same color convention used in the upper panel), and $E_r(\lambda)$ (green dashed line). The black vertical dashed lines connecting both panels show the value of λ where each \mathcal{G}_n has its minimum, λ_n^f . The red dots in the lower panel correspond to $E_n(\lambda_n^f)$.

$0 \leq DO_n(\lambda) \leq 2$. If there are not resonances between λ_L and λ_R , the wave function is roughly independent of λ so $DO_n(\lambda) \simeq 2$. However, the scenario is different when a resonance is present between λ_L and λ_R . In this case, the avoided crossings for a given state Ψ_n are located approximately at λ_L^{av} and λ_R^{av} , where $L(R)$ stands for the leftmost (rightmost) avoided

TABLE I: Resonance Energy obtained by four different methods. Basis size is N=14

λ_{DO}^n		DO	Complex Scaling	Fidelity and Density of States				
				$n = 2$	$n = 3$	$n = 4$	$n = 5$	$n = 6$
1.755 (n=2)	E	-0.99075	-0.99098	-0.99011	—	—	—	—
	α	2.0	2.0	1.560	—	—	—	—
1.8625 (n=3)	E	-0.93427	-0.93452	-0.93434	-0.93383	-0.93303	—	—
	α	2.0	2.0	2.448	1.787	1.414	—	—
2.02 (n=4)	E	-0.85498	-0.85556	-0.85581	-0.85564	-0.85531	-0.85486	—
	α	2.0	2.0	3.339	2.435	1.906	1.519	—
2.255 (n=5)	E	-0.74329	-0.74538	-0.74518	-0.74527	-0.74519	-0.74521	-0.74514
	α	2.0	2.0	4.262	3.098	2.414	1.936	1.574
2.61 (n=6)	E	-0.58276	-0.59077	-0.58825	-0.58910	-0.58942	-0.58965	-0.58979
	α	2.0	2.0	5.248	3.799	3.799	2.373	1.936

crossing. Requesting that $\lambda_L < \lambda_L^{av} < \lambda_R^{av} < \lambda_R$, it follows that $\langle \Psi_n(\lambda_L) | \Psi_n(\lambda_R) \rangle \simeq 0$. With this prescription, the DO_n functions are rather independent of the actual values chosen for λ_L and λ_R . For a given n , $DO_n(\lambda)$ measures how much the state $\Psi_n(\lambda)$ differs from the extended states $\Psi_n(\lambda_R)$ and $\Psi_n(\lambda_L)$.

We look for the states with minimum DO_n , in the same fashion as we did with the fidelity, we can obtain values $E_r(\lambda_{DO}^n) \simeq E_n(\lambda_{DO}^n)$, where λ_{DO}^n is defined by $DO_n(\lambda_{DO}^n) = \min_{\lambda} DO_n(\lambda)$. Figure 5 shows the behavior of DO_n obtained for the same parameters that the ones used in Figure 4, and we compare the values of $E_n(\lambda_{DO}^n)$ with energy values obtained using complex scaling methods in Table I. The curves in Figure 5 show that outside (λ_L, λ_R) the states Ψ_n change very little when λ changes and $DO_n \simeq 1$. Inside the resonance region, $(\lambda_L^{av}, \lambda_R^{av})$, the functions DO_n change abruptly. The width in λ in which a given DO_n changes abruptly apparently depends on the width of the resonance, Γ , but so far we have not been able to relate both quantities.

From Table I and Figure 5 it is rather clear that despite that the fidelity and the DO_n provide approximate values for $E_r(\lambda)$ for different sets of λ 's, both sets belongs to the “same” curve, *i.e.* the same curve considering the numerical inaccuracies. Both methods would give

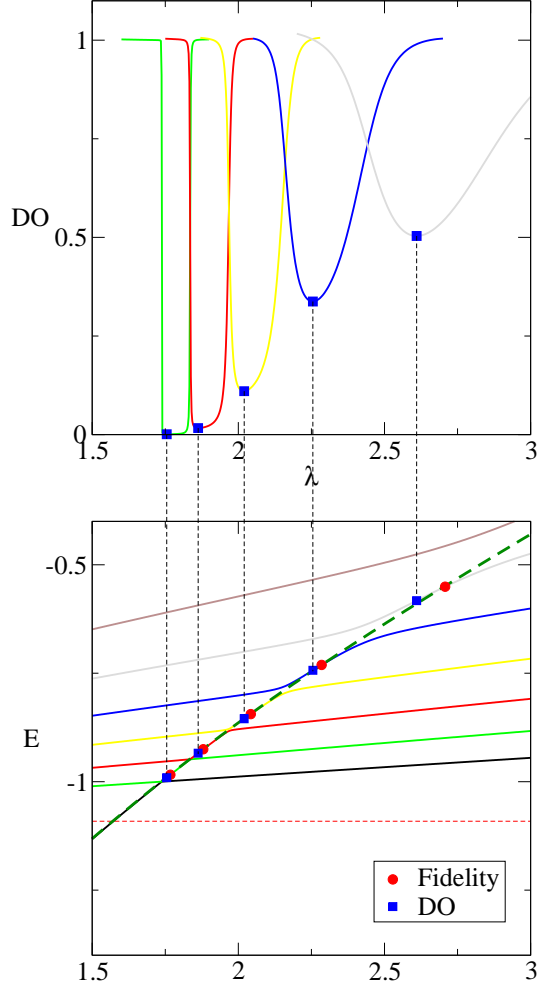


FIG. 5: (color on-line) The lower panel shows the variational energy levels $E_n(\lambda)$, from bottom to top, for $n = 1, \dots, 7$ (the black, green, red, yellow, blue, grey and brown continuous lines, respectively); $E_r(\lambda)$ (the dashed dark green line); $E_n(\lambda_{DO}^n)$ (blue squares) and $E_n(\lambda_n^f)$ (red dots). The upper panel shows the behavior of DO_n vs λ for $n = 2, \dots, 7$. The color convention for the DO_n is the same used in the lower panel. The black dot-dashed vertical lines show the location of the points λ_{DO}^n .

the same results when $|\lambda_R^{av} - \lambda_L^{av}| \rightarrow 0$, but for N finite the fidelity measures how fast the state changes when $\lambda \rightarrow \lambda + \Delta\lambda$ and the DO measures how much a state differs from the extended states located at both sides of the resonance state.

IV. THE ENTROPY

If $\hat{\rho}^{red}$ is the reduced density operator for one electron [19], then the von Neumann entropy \mathcal{S} is given by

$$\mathcal{S} = -\text{tr}(\hat{\rho}^{red} \log_2 \hat{\rho}^{red}), \quad (17)$$

and the linear entropy S_{lin} is given by [11]

$$S_{\text{lin}} = 1 - \text{tr} [(\hat{\rho}^{red})^2], \quad (18)$$

where the reduced density operator is

$$\hat{\rho}^{red}(\mathbf{r}_1, \mathbf{r}'_1) = \text{tr}_2 |\Psi\rangle \langle \Psi|, \quad (19)$$

here the trace is taken over one electron, and $|\Psi\rangle$ is the total two-electron wave function. Both entropies, Eqs. (17) and (18), can be used to analyze how much entanglement has a given state. One can choose between one entropy or the other out of convenience. In this paper we will use the linear entropy. For a discussion about the similarities between the two entropies see Reference [11] and references therein.

As the two electron wave function is not available we instead use the variational approximation Eq. (10). As has been noted in previous works (see [5] and References therein), when the total wave function factorizes in spatial and spinorial components it is possible to single out both contributions, then the analysis of the behavior of the entropy is reduced to the analysis of the behavior of the spatial part S , since the spinorial contribution is constant. In this case, if $\varphi(\mathbf{r}_1, \mathbf{r}_2)$ is the two electron wave function and $\rho^{red}(\mathbf{r}_1, \mathbf{r}'_1)$ is given by

$$\rho^{red}(\mathbf{r}_1, \mathbf{r}'_1) = \int \varphi^*(\mathbf{r}_1, \mathbf{r}_2) \varphi(\mathbf{r}'_1, \mathbf{r}_2) d\mathbf{r}_2, \quad (20)$$

then the linear entropy S_{lin} can be calculated as

$$S_{\text{lin}} = 1 - \sum_i \lambda_i^2, \quad (21)$$

where the λ_i are the eigenvalues of ρ^{red} and are given by

$$\int \rho^{red}(\mathbf{r}_1, \mathbf{r}'_1) \phi_i(\mathbf{r}'_1) d\mathbf{r}'_1 = \lambda_i \phi_i(\mathbf{r}_1). \quad (22)$$

Figure 6 shows the behavior of the linear entropy for several variational levels. The meaning of each curve has been extensively discussed in Reference [19]. We include a brief discussion here for completeness.

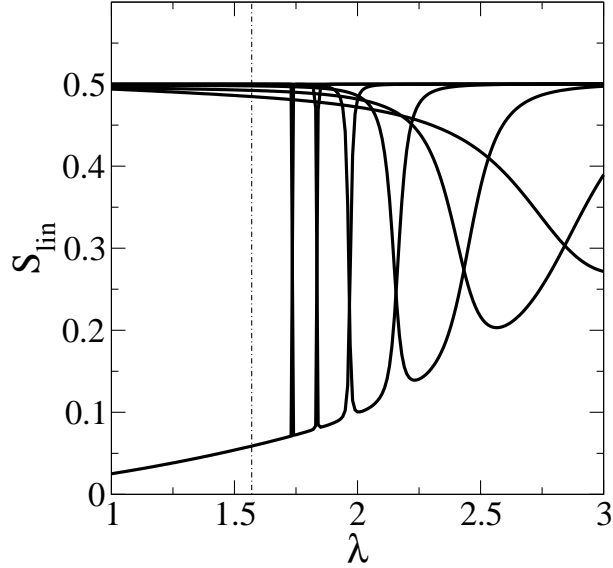


FIG. 6: The figure shows the behavior of $S_{\text{lin}}(\Psi_j^{(\alpha)})$, where the $\Psi_j^{(\alpha)}$ are the variational eigenstates corresponding to the first seven energy levels shown in Figure 1 for $N = 14$ and $\alpha = 2.0$. All the curves $S_{\text{lin}}(\Psi_j^{(\alpha)})$, except for the corresponding to $S_{\text{lin}}(\Psi_1^{(\alpha)})$, have a single minimum located at λ_j^S , *i.e.* $S_{\text{lin}}(\Psi_j^{(\alpha)}(\lambda_j^S)) = \min_{\lambda} S_{\text{lin}}(\Psi_j^{(\alpha)}(\lambda))$. If $i < j$ then $\lambda_i^S < \lambda_j^S$.

When the two-electron quantum dot loses an electron the state of the system can be described as one electron bounded to the dot potential, and one unbounded electron *at infinity*, as a consequence the spatial wave function can be written as a symmetrized product of one electron wave functions so $S_{\text{lin}} = S_c = 1/2$. Therefore if only bound and continuum states are considered the entropy has a discontinuity when λ crosses the threshold value λ_{th} . The picture changes significantly when resonance states are considered. The resonance state keeps its two electrons “bounded” before the ionization for a finite time given by the inverse of the imaginary part of the energy. Of course the life time of a bounded state is infinite while the life time of a resonance state is finite. In reference [19] is suggested that it is possible to construct a smooth function $S(E_r(\lambda))$ that “interpolates” between the minima of the functions $S(\Psi_j)$ shown in Figure 6. This assumption was justified by similar arguments that the used in the present work, *i.e.* if we call λ_n^S to the value of λ where $S(\Psi_n)$ gets its minimum then $E_n(\lambda_n^S)$ follows approximately the curve $E_r(\lambda)$. As Ferrón *et al.* [19] used only one variational parameter α , it seemed natural to pick the minimum value of $S(\Psi_n)$ as the feature that signaled the presence of the resonance state.

Until now we have exploited the fact that $E_r(\lambda)$, at a given λ can be approximated by variational eigenvalues corresponding to different values of the variational parameter, say $E_r(\lambda) \simeq E_n^{(\alpha)}(\lambda) \simeq E_{n'}^{(\alpha')}(\lambda)$ (the superscript α is made evident to remark that the eigenvalues correspond to different variational parameters α and α'). There is no problem in approximating an exact eigenvalue with different variational eigenvalues. But, from the point of view of the entropy, there is a problem since, in general, $S(\Psi_n^{(\alpha)}(\lambda))$ is not close to $S(\Psi_{n'}^{(\alpha')}(\lambda))$. Moreover, as has been stressed in Reference [2], a given numerical method could be useful to accurately calculate the spectrum of a quantum system, but hopelessly inaccurate to calculate the entanglement. In few body systems there is evidence that there is a strong correlation between the entanglement and the Coulombian repulsion between the components of the system [5, 9, 11, 26]. Because of this correlation we will carefully investigate the behavior of the Coulombian repulsion between the electrons in our model.

For the Hamiltonian Eq. (2), and $\psi \in \mathcal{L}^2$ an eigenvector of H with eigenvalue E , the Hellman-Feynman theorem gives that

$$\frac{\partial E}{\partial \lambda} = \langle \psi | \frac{1}{r_{12}} | \psi \rangle. \quad (23)$$

We use both sides of Eq. (23) to analyze how the variational approximation works with expectation values of observables that are not the Hamiltonian. The *r.h.s* of Eq. (23) is well defined if we use \mathcal{L}^2 functions as the approximate variational eigenfunctions.

To evaluate the *l.h.s* of Eq. (23) we take advantage that we have found, independently, the real part of the resonance eigenvalue, $E_r(\lambda)$, using complex scaling methods. Figure 7 shows the behavior of $\frac{dE_r}{d\lambda}$ and the Coulombian repulsion between the two electrons, $\langle \frac{1}{r_{12}} \rangle_n$, where $\langle \dots \rangle_n$ stands for the expectation value calculated with $\Psi_n^{(\alpha)}$. The behavior of $\langle \frac{1}{r_{12}} \rangle_n$ is quite simple to analyze, where the linear entropy of $\Psi_n^{(\alpha)}$ has a valley the expectation value $\langle \frac{1}{r_{12}} \rangle_n$ has a peak. Where the expectation value $\langle \frac{1}{r_{12}} \rangle_n$ has its maximum the corresponding linear entropy has its minimum. The inverse behavior showed by the entropy and the Coulombian repulsion has been observed previously [11, 26].

For a given variational parameter α , and for small n , $\langle \frac{1}{r_{12}} \rangle_n$ has its maximum very close to the curve $\frac{dE_r}{d\lambda}$. Besides, the shape of both curves near the maximum of $\langle \frac{1}{r_{12}} \rangle_n$ is very similar, in this sense our variational approach gives a good approximation not only for $E_r(\lambda)$ but for its derivative too.

For larger values of n the maximum of $\langle \frac{1}{r_{12}} \rangle_n$ gets apart from the curve of $\frac{dE_r}{d\lambda}$, and the

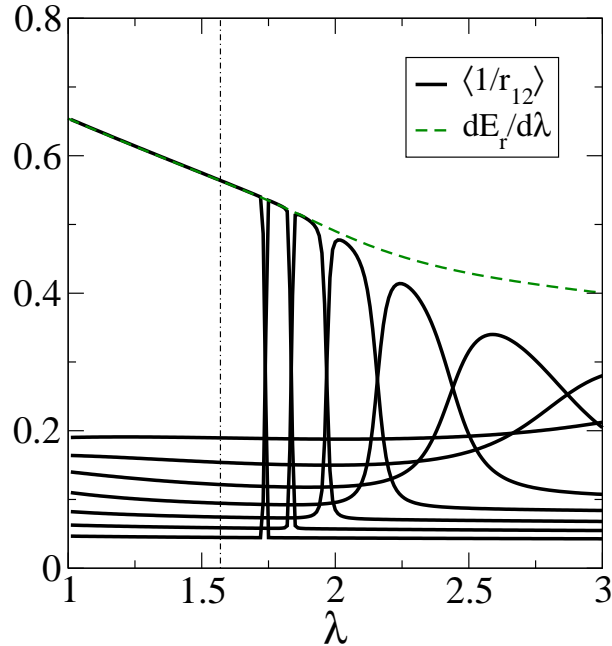


FIG. 7: The figure shows the expectation values of the Coulombian repulsion for the variational states $\Psi_n^{(\alpha)}$, $n = 1, \dots, 8$ with $N = 14$ and $\alpha = 2.0$. Also is showed the curve $\frac{\partial E_r}{\partial \lambda}$ obtained from the complex Energy of the complex scaling method.

shape of the curves near this maximum is quite different. We proceed as before and changing α we obtain a good approximation for $\frac{dE_r}{d\lambda}$ up to a certain value λ_{rep} . For any λ smaller than λ_{rep} , there is a pair n, α such that $\langle \frac{1}{r_{12}} \rangle_{n, \alpha}$ is locally close to $\frac{dE_r}{d\lambda}$ and the slope of both curves is (up to numerical errors) the same, see figure 8.

Apparently there is no way to push further the variational method, at least keeping the same basis set, in order to obtain a better approximation than the depicted in Figure 8. The difficulty seems to be more deep than just a limitation of the variational method used until this point. We can clarify this subject using the properties of the complex scaling method. Let us call ϕ^θ the eigenvector such that

$$H(\theta)\phi^\theta = E_{res}\phi^\theta, \quad (24)$$

where $H(\theta)$ is the Hamiltonian obtained from the complex scaling transformation [29], and θ is the angle of “rotation”. The eigenvector ϕ^θ depends on θ , but for θ large enough the eigenvalue E_{res} does not depend on θ . As pointed by Moiseyev [29], the real part of the expectation value of a complex scaled observable is the physical measurable quantity, while

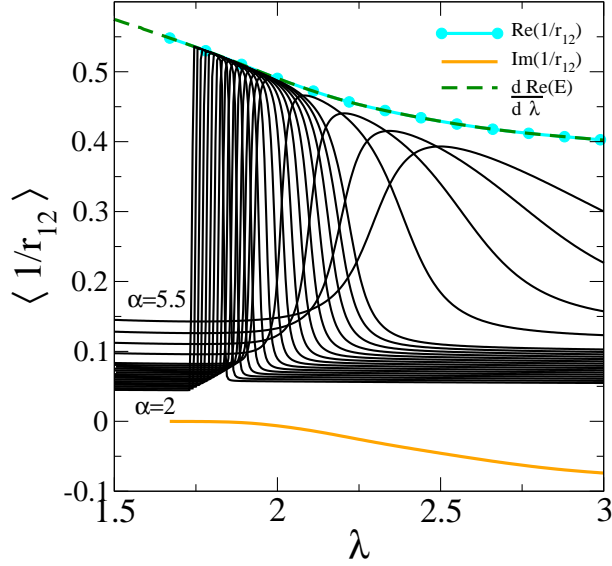


FIG. 8: (color-online) The figure shows the expectation value $\langle 1/r_{12} \rangle_2^{(\alpha)}$ vs. λ for a basis size $N = 14$ and $\alpha = 2, \dots, 3.5$ in 0.1 steps and for $\alpha = 4, \dots, 5.5$ in 0.5 steps (solid black lines). The real (cyan dotted) and imaginary (orange line) parts of $\langle 1/r_{12} \rangle_\theta$ ($\theta = \pi/10$), and the derivative of the real part of the complex-scaled energy are also shown.

the imaginary part gives the uncertainty of measuring the real part. Moreover, the physical measurable quantity must be θ independent as is, for example, the eigenvalue E_{res} .

The eigenvector ϕ^θ can be normalized using that

$$\langle (\phi^\theta)^* | \phi^\theta \rangle = 1. \quad (25)$$

Since ϕ^θ is normalized, we get that

$$\frac{\partial E_{res}}{\partial \lambda} = \langle (\phi^\theta)^* | \frac{e^{-i\theta}}{r_{12}} | \phi^\theta \rangle = \left\langle \frac{1}{r_{12}} \right\rangle_\theta, \quad (26)$$

in this last equation we have used that, under the complex scaling transformation,

$$\frac{1}{r_{12}} \rightarrow \frac{e^{-i\theta}}{r_{12}}, \quad (27)$$

and defined the quantity $\left\langle \frac{1}{r_{12}} \right\rangle_\theta$. This generalized Hellman-Feynman theorem is also valid for Gamow states [30].

Figure 8 shows the behavior of the expectation value in the $\left\langle \frac{1}{r_{12}} \right\rangle_\theta$ as a function of λ . It is clear that the real part of the expectation value $\left\langle \frac{1}{r_{12}} \right\rangle_\theta$ coincides with $\frac{\partial E_r}{\partial \lambda}$. More

interestingly, λ_{rep} is where the imaginary part of $\langle \frac{1}{r_{12}} \rangle_\theta$ became noticeable. From this fact we conclude that it is not possible to adequately approximate the Coulombian repulsion of a resonance state, or its entropy, only with real \mathcal{L}^2 variational functions despite its success when dealing with the resonance state spectrum.

We define the complex scaled density operator of the resonance state by

$$\rho^\theta = |\phi^\theta\rangle\langle(\phi^\theta)^*|, \quad (28)$$

and the complex linear entropy

$$S^\theta = 1 - \text{tr}(\rho_{red}^\theta)^2, \quad (29)$$

where

$$\rho_{red}^\theta = \text{tr}_2 \rho^\theta, \quad (30)$$

and ϕ^θ is the eigenvector of Eq. (24). This definition is motivated by the fact that the density operator should be the projector onto the space spanned by $|\phi^\theta\rangle$. As the normalization Eq. (25) requires the *bra* to be conjugated, then ρ^θ is the adequate projector to use.

Because of the normalization, Eq. (25), we have that $\text{tr} \rho^\theta = \text{tr} \rho_{red}^\theta = 1$ *despite that both density operators have complex eigenvalues.*

Figure 9 shows that up to certain value of λ the real part of S^θ follows closely a envelope containing the minima of the functions $S(\Psi_n)$. However, for λ large enough, S^θ gets apart from the functions $S(\Psi_n)$. It is worth to mention that for θ large enough S^θ **does not depend on θ** . On the other hand, far away from the threshold, the complex scaling requires larger values of θ to isolate the resonance state eigenenergy, but in this regime the method becomes unstable. Because of the numerical evidence, near the threshold the entropy calculated by Ferrón *et al.* is basically correct, but for larger values of λ the amount of entanglement of the resonance state should be characterized by S^θ and not by any of the $S(\Psi_n)$.

V. SUMMARY AND CONCLUSIONS

We have presented numerical calculations about the behavior of the fidelity and the double orthogonality functions $DO_n(\lambda)$. The numerical results show that it is possible to obtain $E_r(\lambda)$ with great accuracy, for selected values of λ , without employing any stabilization

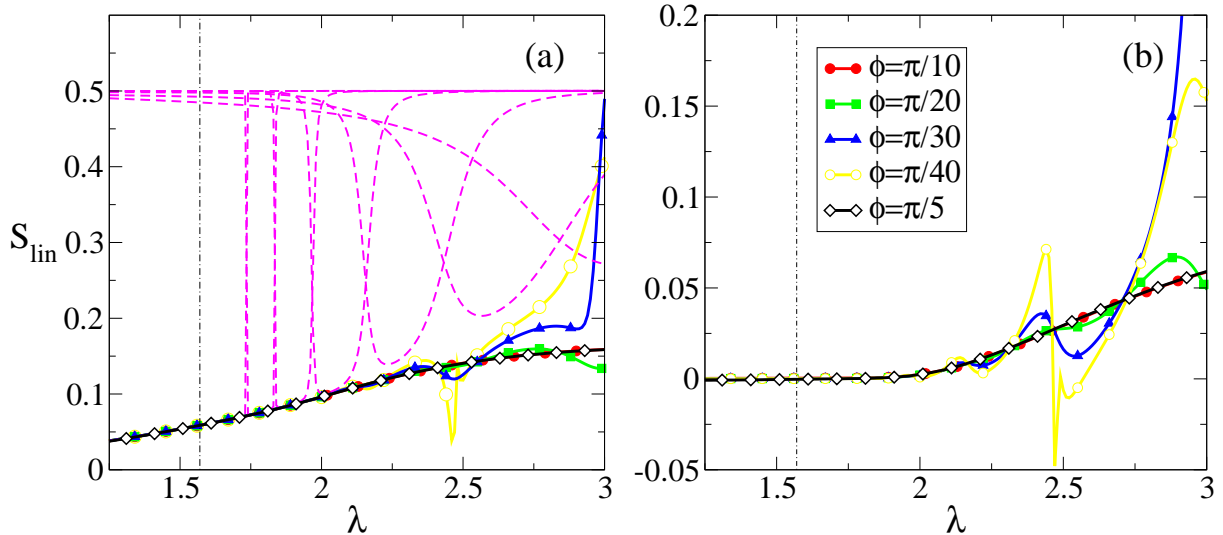


FIG. 9: (color-online) Figure (a) shows the linear entropy for the same values as in figure 6 (magenta dashed lines). Also showed is the real part of the complex linear entropy for several values of the complex rotation angle $\theta = \frac{\pi}{5}, \frac{\pi}{10}, \frac{\pi}{20}, \frac{\pi}{30}, \frac{\pi}{40}$ (black empty diamonds, red dots, green squares, blue triangle, yellow empty dots). Figure (b) shows the imaginary part of the complex linear entropy for the same values as in (a).

method. These two methods to find $E_r(\lambda)$ do not depend on particular assumptions about the model or the variational method used to find approximate eigenfunctions above the threshold, their success depends on the ability of the approximate eigenstates to detect the non-analytical changes in the spectrum.

The fidelity has been extensively used to detect quantum phase transitions in spin systems [20], the behavior of quasi-integrable systems [31], thermal phase transitions [32], etc. To the best of our knowledge this work is the first attempt to apply the concept of fidelity to resonance states and to the characterization of spectral properties of a system with non-normalizable eigenstates. Besides, it is remarkable that the fidelity and the double orthogonality give the real part of the resonance eigenvalue using only real variational functions. This energy as a function of λ is obtained by moving the nonlinear parameter α but *without* fitting as needed by standard stabilization methods. Moreover, as shown by the tabulated values in Table I the fidelity provides $E_r(\lambda)$ as accurately as the density of states method, with considerable less numerical effort.

We proposed a definition of the resonance entropy based on a complex scaled extension of

the usual definition. The extension implies that the reduced density operator is not hermitian and has complex eigenvalues, resulting in a complex entropy. The real and imaginary parts of the complex entropy are θ independent, as should be expected for the expectation value of an observable [29]. This independence gives support to the interpretation of the real part of the entropy as the amount of entanglement of the resonance state.

Other kinds of resonances, as those that arise from perturbation of bound states embedded in the continuum, could be studied applying the same quantum information methods used in this paper. Work is in progress in this direction.

Acknowledgments

We would like to acknowledge SECYT-UNC, CONICET and FONCyT for partial financial support of this project.

-
- [1] A. Osterloh, L. Amico, G. Falci, and R. Fazio, *Nature* **416**, 608 (2002).
 - [2] Norbert Schuch, Michael M. Wolf, Frank Verstraete, and J. I. Cirac, *Phys. Rev. Lett.* **100**, 030504 (2008).
 - [3] W. K. Wootters, *Phys. Rev. Lett* **80**, 2245 (1998).
 - [4] Longyan Gong and Peiqing Tong, *Phys. Rev. B* **78**, 115114 (2008); Wing-Chi Yu, Ho-Man Kwok, Junpeng Cao, and Shi-Jian Gu, *Phys. Rev. E* **80**, 021108 (2009); David Schwandt, Fabien Alet, and Sylvain Capponi, *Phys. Rev. Lett.* **103**, 170501 (2009).
 - [5] O. Osenda and P. Serra, *Phys. Rev. A* **75**, 042331 (2007).
 - [6] O. Osenda and P. Serra, *J. Phys. B: At. Mol. Opt. Phys.* **41**, 065502 (2008).
 - [7] F. Schmüser and Dominik Janzing, *Phys. Rev. A* **73**, 052313 (2006).
 - [8] Yan Liu, Yujun Zheng, Weiyi Ren, and Shiliang Ding, *Phys. Rev. A* **78**, 032523 (2008).
 - [9] J. P. Coe, A. Sudbery, and I. D'Amico, *Phys. Rev. B* **77**, 205122 (2008).
 - [10] Clive Emary, *Phys. Rev. B* **80**, 161309(R) (2009); Robert Roloff and Walter Pötz, *Phys. Rev. B* **76**, 075333 (2007).
 - [11] S. Abdullah, J.P. Coe, and I. D'Amico, *Phys. Rev. B* **80**, 235302 (2009).
 - [12] L. Sælen, R. Nepstad, I. Degani, and J. P. Hansen, *Phys. Rev. Lett.* **100**, 046805 (2008).

- [13] Daniel Loss and David P. DiVincenzo, *Phys. Rev. A* **57**, 120 (1998).
- [14] A. Imamoglu, D.D. Awschalom, G. Burkard, D.P. DiVincenzo, D. Loss, M. Sherwin, and A. Small, *Phys. Rev. Lett.* **83**, 4204 (1999).
- [15] W. P. Reinhardt and Seungsuk Han, *International Journal of Quantum Chemistry* **57**, 327 (1996).
- [16] Y. Sajeev, and N. Moiseyev, *Phys. Rev. B* **78**, 075316 (2008).
- [17] M. Bylicki, W. Jaskólski, A. Stachów, and J. Diaz, *Phys. Rev. B* **72**, 075434 (2005).
- [18] J. Dubau, and I. A. Ivanov, *J. Phys. B: At. Mol. Opt. Phys.* **31** 3335 (1998).
- [19] A. Ferrón, O. Osenda and P. Serra, *Phys. Rev. A* **79**, 032509 (2009).
- [20] P. Zanardi and N. Paunković, *Phys. Rev. E* **74**, 031123 (2006).
- [21] P. Zanardi, P. Giorda, and M. Cozzini, *Phys. Rev. Lett.* **99**, 100603 (2007).
- [22] S. Garnerone, N. T. Jacobson, S. Haas, and P. Zanardi, *Phys. Rev. Lett.* **102**, 057205 (2009).
- [23] A.T. Kruppa and K. Arai, *Phys. Rev. A* **59**, 3556 (1999).
- [24] F. M. Pont and P. Serra, *J. Phys A: Math. Theor.* **41**, 275303 (2008).
- [25] A. Galindo and P. Pascual. *Quantum Mechanics I* (Eudema, 1989).
- [26] O. Osenda, P. Serra and S. Kais, *International Journal of Quantum Information* **6**, 303 (2008).
- [27] P. Serra and S. Kais, *Chem. Phys. Lett.* **372**, 205 (2003).
- [28] Sabyasachi Kar and Y. K. Ho, *J. Phys. B: At. Mol. Opt. Phys.* **37**, 3177 (2004).
- [29] N. Moiseyev, *Phys. Rep.* **302**, 211(1998).
- [30] P. Ziesche, K. Kunze and B. Milek, *J. Phys. A: Math. Gen.* **20**, 2859(1987).
- [31] Yaakov S. Weinstein and C. S. Hellberg, *Phys. Rev. E* **71**, 016209 (2005).
- [32] H. T. Quan and F. M. Cucchietti, *Phys. Rev. E* **79**, 031101 (2009).
- [33] V. A. Mandelshtam, T. R. Ravuri and H. S. Taylor, *Phys. Rev. Lett.* **70**, 1932 (1993).